Waveguide integration of a > 4.7-THz quantum-cascade laser

Eleanor Nuttall,[1,✉] Yingjun Han,[1] Diego Pardo,[2] Sanchit S. Kondawar,[1] Nick Brewster,[2] Mohammed Salih,[1] Lianhe Li,[1] Michael D. Horbury,[1] A. Giles Davies,[1] Edmund H. Linfield,[1] Hui Wang,[2] Paul Dean,[1] Brian N. Ellison,[2] and Alexander Valavanis[1]

[1] *School of Electronic and Electrical Engineering, The University of Leeds, Leeds, LS2 9JT, UK*

[2] *UKRI–STFC Rutherford Appleton Laboratory, Harwell Oxford, Didcot, OX11 0QX, UK*

✉ E-mail: cm14en@leeds.ac.uk

Waveguide integration of terahertz quantum cascade lasers (THz QCLs) is demonstrated at frequencies above 4.7 THz. A precision micromachining technique, followed by diamond-turning and electroless-plating has been used to manufacture hollow rectangular waveguides with integrated diagonal feedhorns. It is shown that surface roughness at the ≈ 1 μm level is achieved, enabling outcoupling of radiation in the 4.75–5.05 THz band, with a divergence angle of < 5° along the plane of the QCLs substrate.

Introduction: THz QCLs are compact, yet powerful semiconductor sources of radiation in the ≈1.2–5-THz band of the electromagnetic spectrum [1, 2]. These devices have a wide range of potential applications, including atmospheric and space research [2], owing to their high emission intensity, narrow intrinsic linewidths, and compact size. However, integration of THz QCLs with other system components is challenging, both in terms of near-field coupling to external waveguides, and far-field quasi-optical coupling to external devices.

The gain medium of a THz QCL consists of a stack of semiconductor layers, grown using molecular-beam epitaxy (MBE) to a total thickness of ≈ 10 μm, and enclosed within a plasmonic waveguide structure. The electromagnetic mode profile across the laser facet is, therefore, considerably narrower than the ≈ 100-μm free-space emission wavelength. This results in a widely divergent and non-Gaussian far-field beam pattern [3], which is challenging to couple into external devices. This can be mitigated partially, through photonic engineering approaches and custom assemblies of quasi-optical components (e.g., ref. [4]).

Alternatively, direct (near-field) coupling between components is a more attractive option for application environments, such as satellite payloads, in which the system volume, mass and mechanical robustness are key constraints. However, the dimensional tolerances required for manufacturing waveguides and the coupling interfaces become extremely challenging as the THz frequency of the source increases. Nevertheless, some progress has been made. Monolithic semiconductor fabrication processes have been used to integrate 2.8-THz QCLs with Schottky mixers [5], and 3.4-THz QCLs with modulators [6]. We have also previously embedded 3.5-THz QCLs into precision micromachined metallic waveguides, which are optically out-coupled to diagonal feedhorns [7]. It is though, desirable to extend these approaches to exploit the highest achievable frequency range of QCLs, up to around ≈ 5-THz. For example, 4.7-THz QCLs are required for radiometric observations of atomic oxygen [9]. However, the 34% reduction in wavelength from 3.5 to 4.7 THz requires a similar improvement in the machining tolerances to achieve comparable waveguide performance.

In this work, we demonstrate the first such high-frequency waveguide integration of a QCL, emitting in the 4.7–5.1-THz band. We achieve this through a combination of precision milling, diamond-turned surface finishing and electroless gold plating. Compared to standard gold plating, we have achieved an order-of-magnitude reduction in gold grain size to ≈ 1μm , enabling successful propagation and outcoupling of THz radiation. The following sections describe the fabrication of the QCL and its waveguide enclosure, and characterisation of its optical and thermal performance.

Device fabrication: The QCL active region was based on a ≈ 4.7-THz GaAs/AlGaAs phonon-enhanced bound-to-continuum design [9], which was grown using molecular-beam epitaxy to a thickness of 12 μm. The device was then processed into a gold–gold double-metal plasmonic ridge-waveguide configuration, with a transverse ridge width of 60 μm, and with the substrate thickness reduced to 88 μm, using a combination of wet chemical etching and mechanical lapping processes. The device was cleaved to a length of 1200 μm, and diced using a diamond wafer-saw, to a chip of width ≈ 200 μm.

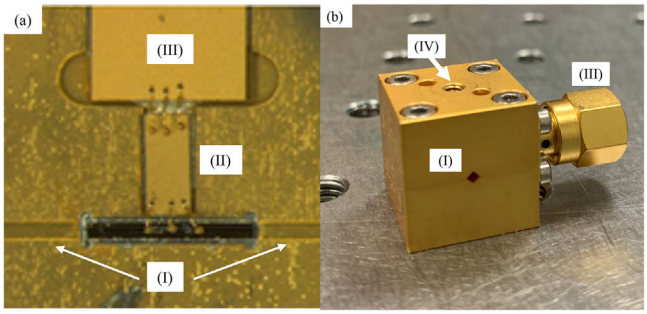

Fig. 1 *Structure of QCL waveguide module, showing (a) photograph of the interior of the assembled module, and (b) photograph of the exterior of the assembled module. Labels show (I) waveguide channels, terminated with diagonal feedhorns, (II) QCL mounted within recess, (III) SMA connector and internal bonding point and (IV) mounting point for external temperature probe*

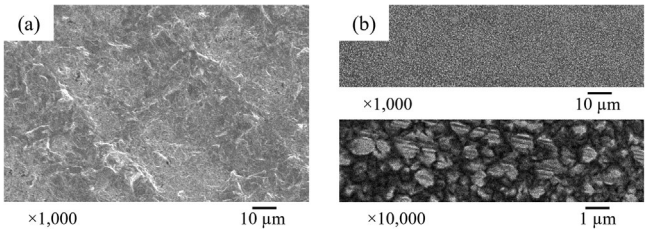

Fig. 2 *Scanning electron micrographs of surface-finishing tests on oxygen-free copper, using (a) standard gold plating process at 1000× magnification, and (b) electroless gold-plating and diamond turning process, at 1000× and 10,000× magnification*

An external waveguide enclosure with diagonal feedhorns was fabricated for the QCL, using a split-block machining approach [10]. This feedhorn geometry allows strong coupling of radiation into the fundamental Gaussian mode, while being much simpler to fabricate than structures such as corrugated conical feedhorns. A pair of oxygen-free copper blocks, each with base area of (15 × 15) imm^2 and a height of 7.5mm were used to form the enclosure. Rectangular channels with widths and depths of 170 μm and 40 μm, respectively were precision machined into each block, as shown in Figure 1a using a KERN mill. The two blocks were aligned using precision dowels, such that they co-registered to form a complete enclosure, containing a hollow rectangular waveguide with a cross-sectional area of (170 × 80) μm^2 (Figure 1b). Although this waveguide is overmoded at 4.7-THz, it eases manufacturing difficulty, and provides a useful intermediate step towards a fundamental IEEE WM-57 standard waveguide. A diagonal feedhorn with an across-diagonal aperture of (1.56 × 1.56)-mm^2 was milled into each channel with a slant angle of 7.5°. An additional recessed area, with a 1600 μm length and 250 μm width, was milled into the centre of the lower channel, to house the QCL.

A set of surface-finishing steps was undertaken to achieve good performance at >4.7-THz. The surface of each block was finished using a Precitech Nanoform X single-point diamond turning lathe, to achieve a surface roughness on the scale of ≈10 nm. The surfaces of the copper blocks were then finished with a gold electroless plating process, resulting in a gold grain size on the scale of ≈ 1 μm. For comparison, an equivalent electroplating process was found to yield ≈ 10 μm roughness, as shown in Figure 2. The QCL was solder-mounted into the recessed area and wire-bonded to an integrated electrical SMA connector via an intermediate thermal-isolation heatsink, prior to final assembly of the waveguide module.

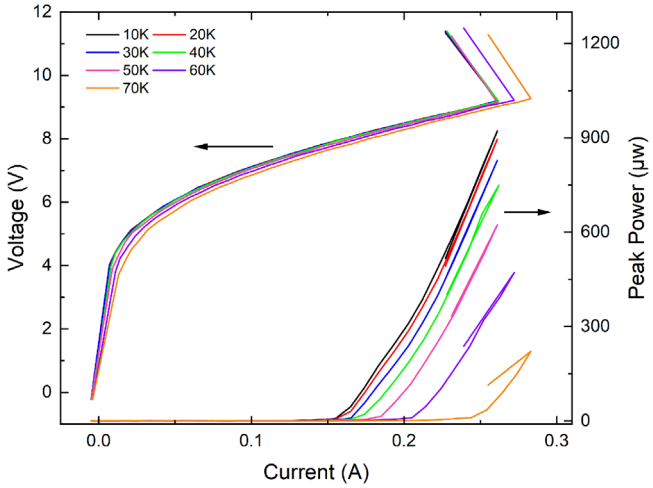

Fig. 3 *Light–current–voltage measurements of the 4.7-THz waveguide-integrated QCL at a 2% duty cycle between 10 and 70 K*

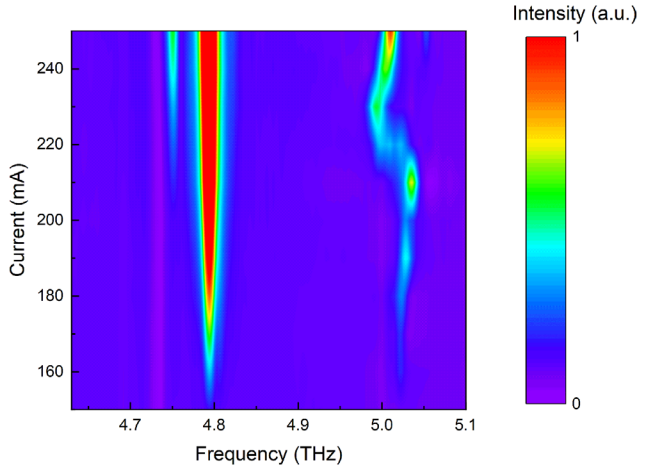

Fig. 4 *FTIR spectrum of the waveguide-integrated QCL at a range of drive currents. Normalised spectral intensity is shown on a linear colour-scale*

Device characterisation: The QCL was mounted on the cold-finger of a Janis ST-100 liquid-helium cryostat, and driven using an Agilent 8114A high-current pulse generator (2% duty cycle; 10 kHz repetition rate). This current pulse train was externally gated using a 167-Hz square-wave envelope, and the emitted THz radiation was coupled into a helium-cooled bolometric detector using a pair of off-axis paraboloidal mirrors. A lock-in amplifier, referenced to the pulse envelope, was used to record the bolometric signal as a function of QCL drive current, as shown in Figure 3. A threshold current of 160 mA was observed at low heatsink temperatures (current density, $J_{\text{th}} = 220$ A cm^{-2}) and a maximum operating temperature of 70 K was determined. An estimated peak output power of $\sim 920\,\mu$W was inferred from the (uncalibrated) detector responsivity.

These results are comparable to those obtained from an equivalent unmounted device grown from the same wafer, and cleaved to a similar length of 1500 μm. This device had a threshold current density of 210 A cm^{-2} at 10 K, a maximum operating temperature of 80 K and a peak output power of 1.2 mW. Although there is a slight reduction in pulsed performance, these comparisons indicate a generally successful optical integration and outcoupling from the waveguide module.

The emission spectrum of the QCL was recorded using a Bruker Fourier Transform Infrared (FTIR) spectrometer, at a range of drive currents, as shown in Figure 4. Multimode emission was observed, with principal lines seen at 4.749, 4.789 and 5.010 THz.

The potential for operation at high duty cycle (or continuous wave) was assessed by recording the peak output power of the laser, as a function of the duty cycle of the power supply, with the QCL operating at a bias of 250 mA. Figure 5 shows that the emitted THz power decreases as duty-cycle increases, owing to internal Joule heating within the QCL

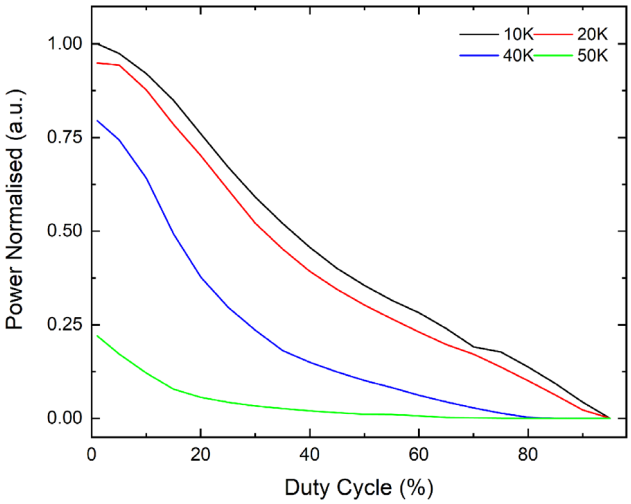

Fig. 5 *Output power of the waveguide-integrated QCL as a function of duty cycle, at a fixed bias of 250 mA. Results are shown for a range of heatsink temperatures*

active region. Nevertheless, emission is achieved up to 90% duty cycle at 10 K.

The difference between the internal temperature of the QCL active region T_{QCL} and the measured heatsink temperature T_{HS} can be approximated by a linear thermal resistance model:

$$\Delta T = T_{\text{QCL}} - T_{\text{HS}} \approx IV\gamma R_{\text{th}} \tag{1}$$

where I is the peak QCL drive current, V is the voltage dropped across the laser, γ is the duty cycle, and R_{th} is the thermal resistance between the QCL active region and the heat sink.

At low duty cycles, Joule heating is negligible, and therefore $T_{\text{QCL}} \approx T_{\text{HS}}$. As such, the low duty-cycle output power in Figure 3 may be used as a thermometric property, allowing the internal temperature of the QCL to be inferred at higher duty cycles from Figure 5.

The thermal resistance between the QCL and the heatsink was calculated as 31 K/W, at 10 K heat-sink temperature and at a drive current of 250 mA. As a result, a d.c. bias on the QCL leads to an inferred internal temperature of $T_{\text{QCL}} \approx 90$ K, which exceeds the maximum operating temperature of the device. For comparison, the equivalent non-integrated QCL was able to operate in continuous-wave mode up to a temperature of 62 K, with a maximum output power of 160 μW at low heatsink temperatures. A thermal resistance of 7 K/W was inferred for the non-integrated device.

Although the reason for this increased thermal resistance has not been identified definitively, we believe that the difficulty in obtaining a uniform solder coverage within the deep waveguide recess may contribute to the issue. Improvements in the solder-mounting between the QCL and the waveguide module, and in the heat-sink design could potentially reduce the thermal resistance and enable continuous-wave operation.

Beam profile analysis: The far-field beam divergence was measured from each feedhorn using a knife-edge technique. The QCL was driven in pulsed mode at a current of 240 mA with an 8% duty-cycle, and at a heat-sink temperature of 10 K to obtain maximal output power. The beam was coupled into a bolometric detector using a pair of paraboloidal mirrors, as described previously.

A knife edge was placed in the divergent part of the QCL emission, at a distance of 110 mm from the feedhorn aperture. The calculated Fraunhofer range was 78 mm for the QCL emission wavelength, and feedhorn aperture size. The power coupled into the detector was recorded as the knife edge was scanned progressively through the beam at 1 mm intervals. This was then differentiated to obtain the profile of the beam, as shown in Figure 6. Repeated measurements were taken with the knife edge moving in the directions parallel and perpendicular to the interface between the two halves of the split-block structure, and for each feedhorn.

The angles of divergence were 4.5° and 4.9° for the front feedhorn in the perpendicular and parallel directions respectively, and 6° for the

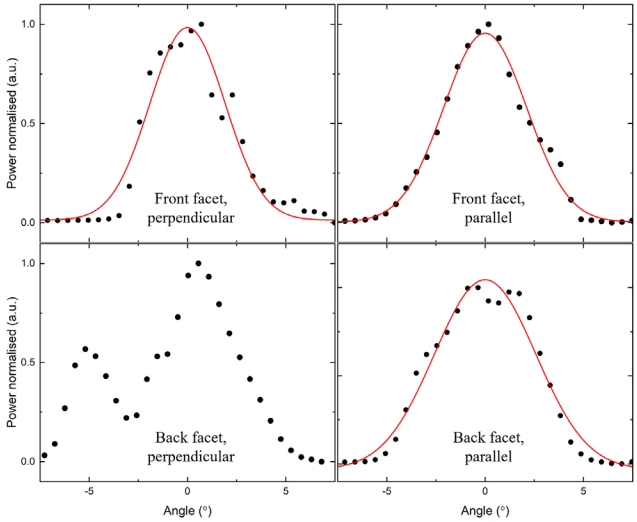

Fig. 6 *Derivative plots of knife-edge measurements of far-field beam profiles of integrated 4.7-THz QCL, for the front facet (top) and back facet (bottom) in the perpendicular plane (left) and parallel plane (right) of the waveguide block*

parallel direction of the back feedhorn. These values are somewhat larger than the analytical value calculated for a uniform field across a square aperture, 2.9°, indicating that the near field is confined to a narrower region within the aperture. The larger back-feedhorn divergence is likely to be a combination of alignment of the QCL within the waveguide and resulting differences in the near-field mode, and experimental uncertainty in the measurement of the knife-edge distance from the feedhorn.

The perpendicular profile for the back facet showed strong dual-lobed behaviour and therefore the angle of divergence is poorly defined.

Although a diagonal horn is expected to yield a single-lobed emission, the split-block geometry induces a conductivity defect in the perpendicular direction, and hence a phase shift in the near-field. At >4.7 THz, the size of this defect may be significant enough to result in a splitting of the far-field pattern, offering a potential explanation for the observed anomalous pattern.

As QCL emission results from intersubband transitions, the polarisation is expected to be linear. However, an ellipticity of $R = 1.6$ was determined from a measurement of the front feedhorn using a pair of Microtech G50 wire-grid polarizers, implying that the waveguide structure results in some depolarisation of the QCL beam.

Conclusion: We have demonstrated the successful fabrication and integration of a >4.7-THz QCL into a waveguide cavity—the highest frequency waveguide integrated THz QCL to date. A reduction in surface-roughness in the external waveguide structure was achieved through diamond-turning and electro-less plating, enabling pulsed QCL operation up to 70 K, or up to 90% duty cycle at low temperature. A low beam divergence was observed, on the scale of <5°, matching the level achievable with complex facet-patterning techniques. However, the dual-lobed emission profile may introduce challenges for far-field coupling to external devices. Future work will be on improvements in thermal management, and in feedhorn design to achieve single-lobed, continuous-wave emission.

Author contributions: Eleanor Nuttall: Investigation, visualization, writing - original draft. Yingjun Han: Investigation, methodology, writing - review and editing. Diego Pardo: Conceptualization, investigation, methodology. Sanchit Kondawar: Investigation. Nick Brewster: Resources. Mohammed Salih: Investigation. Lianhe Li: Resources. Michael Horbury: Investigation. Giles Davies: Conceptualization, funding acquisition. Edmund Linfield: Conceptualization, funding acquisition. Hui Wang: Conceptualization, funding acquisition. Paul Dean: Conceptualization, funding acquisition, supervision. Brian Ellison: Conceptualization, funding acquisition, supervision. Alexander Valavanis: Conceptualization, funding acquisition, investigation, project administration, supervision, writing - review and editing.

Acknowledgements: This work has been supported by UK Space Agency (Future Leaders Fellowship NSTP3-FT2-002), the Royal Society (General Support Technology Programme contract WM150029), the European Space Agency (contract 4000114487/15/NL/AF), the Centre for Earth Observation Instrumentation (Fast Track contract RP10G0435A03), the Engineering and Physical Sciences Research Council (Wolfson Research Merit Award EP/P021859/1) and the UK Research and Innovation (Programme grant MR/S016929/1).

Conflict of interest: The authors declare no conflict of interest.

Data availability statement: The data that support the findings of this study are openly available in the Research Data Leeds repository at https://doi.org/10.5518/1141, reference number 1141.

Received: *10 May 2022* Accepted: *11 December 2022*
doi: 10.1049/ell2.12703

References

1 Köhler, R., Tredicucci, A., Beltram, F., Beere, H.E., Linfield, E.H., Davies, A.G., Ritchie, D.A., Iotti, R.C., Rossi, F.: Terahertz semiconductor-heterostructure laser. *Nature* **417**, 156–159 (2002). https://doi.org/10.1038/417156a

2 Hübers, H.W., Pavlov, S., Semenov, A., Köhler, R., Mahler, L., Tredicucci, A., Beere, H.E., Ritchie, D.A., Linfield, E.H.: Terahertz quantum cascade laser as local oscillator in a heterodyne receiver. *Opt. Express* **13**(15), 5890–5896 (2005). https://doi.org/10.1364/OPEX.13.005890

3 Adam, A.J.L., Kašalynas, I., Hovenier, J.N., Klaassen, T.O., Gao, J.R., Orlova, E.E., Williams, B.S., Kumar, S., Hu, Q., Reno, J.L.: Beam patterns of terahertz quantum cascade lasers with subwavelength cavity dimensions. *Appl. Phys. Lett.* **88**(15), 151105 (2006). https://doi.org/10.1063/1.2194889

4 Miao, W., Lou, Z., Xu, G.-Y., Hu, J., Li, S.-L., Zhang, W., Zhou, K.-M., Yao, Q.-J., Zhang, K., Duan, W.-Y., Shi, S.-C., Colombelli, R., Beere, H.E., Ritchie, D.A.: Demonstration of a fully integrated superconducting receiver with a 2.7 THz quantum cascade laser. *Opt. Express* **23**, 4453–4458 (2015). https://doi.org/10.1364/OE.23.004453

5 Wanke, M.C., Young, E.W., Nordquist, C.D., Cich, M.J., Grine, A.D., Fuller, C.T., Reno, J.L., Lee, M.: Monolithically integrated solid-state terahertz transceivers. *Nat. Photonics* **4**(8), 565–569 (2010). https://doi.org/10.1038/nphoton.2010.137

6 Kundu, I., Freeman, J.R., Dean, P., Li, L.H., Linfield, E.H., Davies, A.G.: Terahertz photonic integrated circuit for frequency tuning and power modulation. *Opt. Express* **28**(4), 4374–4386 (2020). https://doi.org/10.1364/OE.380656

7 Ellison, B.N., Valavanis, A., Auriacombe, O., Gerber, D., Rawlings, T., Brewster, N., Oldfield, M.L., Han, Y., Li, L.H., Zafar, E., Linfield, E.H., Davies, A.G., Savini, G., Emes, M., Winter, B., Walker, D., Saenz, E.: 3.5 THz quantum-cascade laser emission from dual diagonal feedhorns. *Int. J. Microwave Wireless Technolog.* **11**, 909–917 (2019). https://doi.org/10.1017/S175907871900028X

8 Richter, H., Buchbender, C., Güsten, R., Higgins, R., Klein, B., Stutzki, J., Wiesemeyer, H., Hübers, H.-W.: Direct measurements of atomic oxygen in the mesosphere and lower thermosphere using terahertz heterodyne spectroscopy. *Commun. Earth Environ.* (1), 1–9 (2021). https://doi.org/10.1038/s43247-020-00084-5

9 Schrottke, L., Wienold, M., Sharma, R., Lü, X., Biermann, K., Hey, R., Hübers, H.-W., Grahn, H.T.: Quantum-cascade lasers as local oscillators for heterodyne spectrometers in the spectral range around 4.745 THz. *Semicond. Sci. Technol.* **28**(3), 035011 (2013). https://doi.org/10.1088/0268-1242/28/3/035011

10 Johansson, J.F., Whyborn, N.D.: The diagonal horn as a sub-millimeter wave antenna. *IEEE Trans. Microwave Theory Tech.* **40**(5), 795–800 (1992). https://doi.org/10.1109/22.137380